SUPPORTING INFORMATION

Tracking Catalyst Redox States and Reaction Dynamics in Ni-Fe Oxyhydroxide Oxygen Evolution Reaction (OER) Electrocatalysts: The Role of Catalyst Support and Electrolyte pH

Mikaela Görlin[†‡], Jorge Ferreira de Araújo[†], Henrike Schmies[†], Denis Bernsmeier[†], Sören Dresp[†], Manuel Gliech[†], Zenonas Jusys[§], Petko Chernev[‡], Ralph Kraehnert†, Holger Dau[‡], Peter Strasser[†]

[†] Department of Chemistry, Chemical Engineering Division, Technical University of Berlin, Straße des 17. June 124, 10623, Berlin, Germany

[‡] Department of Physics, Free University of Berlin, Arnimallee 14, 14195 Berlin, Germany

[§] Institute of Surface Chemistry and Catalysis, Ulm University, Albert-Einstein-Allee 47, 89081, Ulm, Germany

S3.1. Physical Characterization of Ni-Fe Catalysts

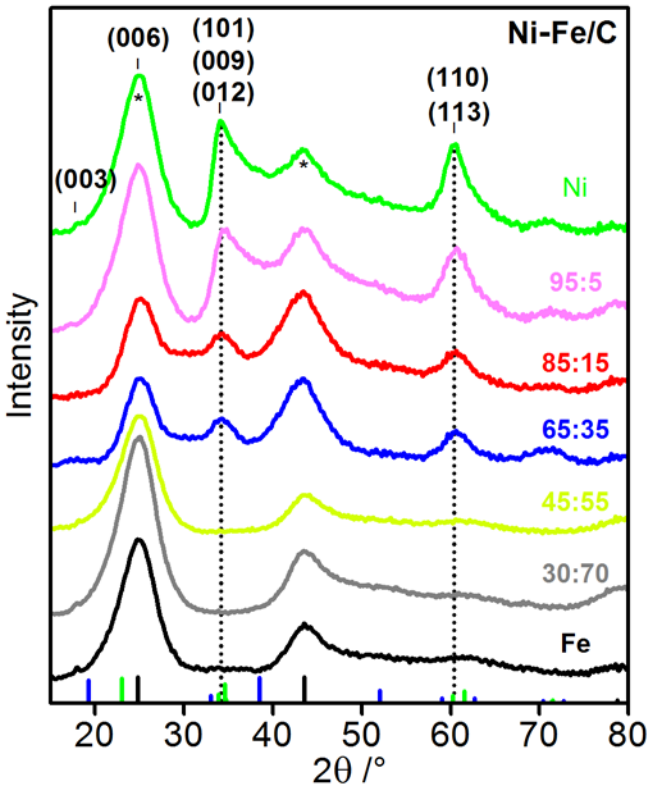

Figure S1. Powder X-ray diffraction of carbon supported Ni-Fe/C catalysts supported on Vulcan XC-72r with various Ni:Fe stochiometries. The catalyst composition is indicated as at. % Fe. The bottom lines show pdf reference patterns of α-$Ni(OH)_2$ *(green)*, pdf # 00-038-0715, β-$Ni(OH)_2$ (*blue)*, pdf # 01-074-2075, and of carbon (*black*).

S3.2. Electrocatalytic Oxygen Evolution Activity

Steady-state vs potential cycling

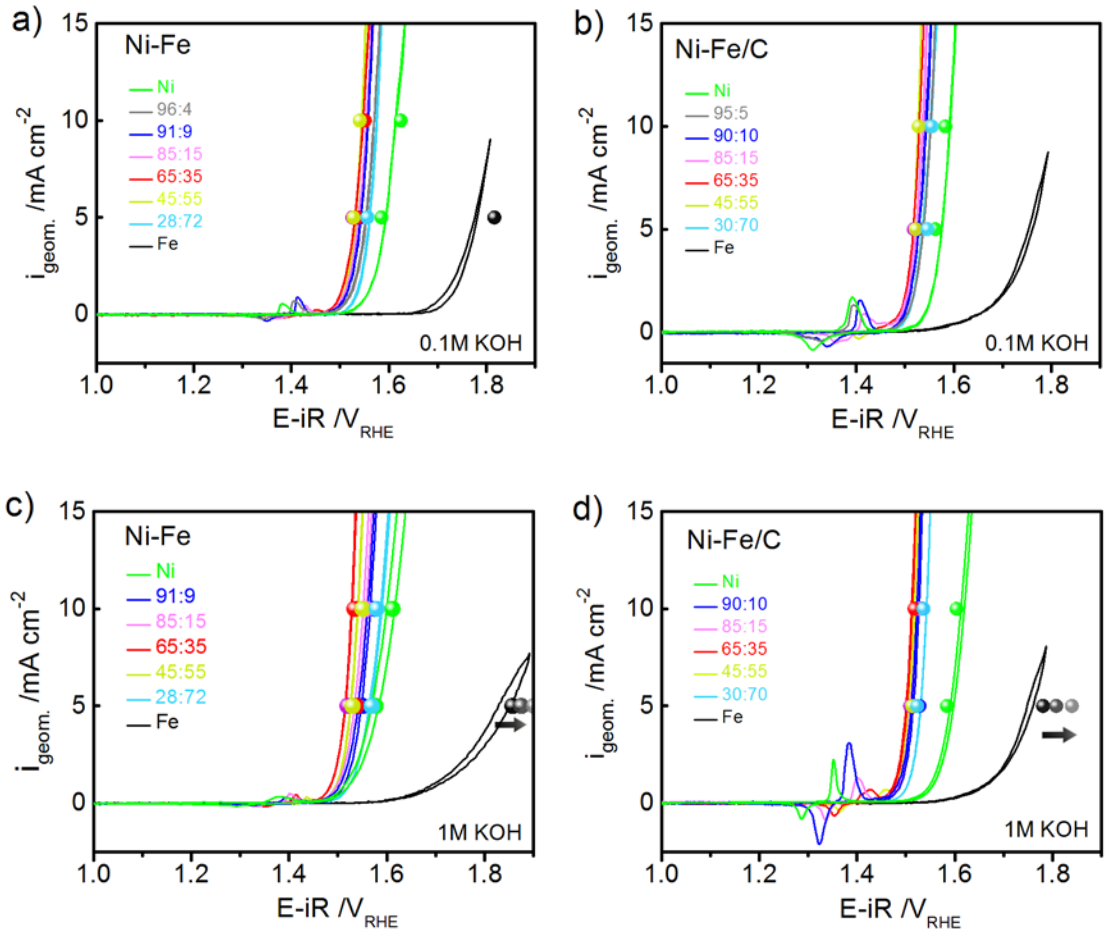

Figure S2. CVs measured at scan rate of 2 mV/s *(curves)* and steady-state chronopotentiometric measurements *(circles)* **(a)** unsupported Ni-Fe catalysts in 0.1 M KOH **(b)** Carbon supported Ni-Fe/C catalysts in 0.1 M KOH. **(c)** Ni-Fe catalysts in 1 M KOH **(d)** Ni-Fe/C catalysts in 1 M KOH. The CVs were recorded at a scan rate of 1600 rpm and the steady-state measurements at a rotation speed of 2200 rpm to avoid bubble blockage at the electrode surface. The metal loadings of Ni+Fe were kept at ~10 µg cm^{-2}, determined prior to the measurements by ICP-OES. The Ni:Fe compositions are indicated in the legends as at. %.

Tafel slopes

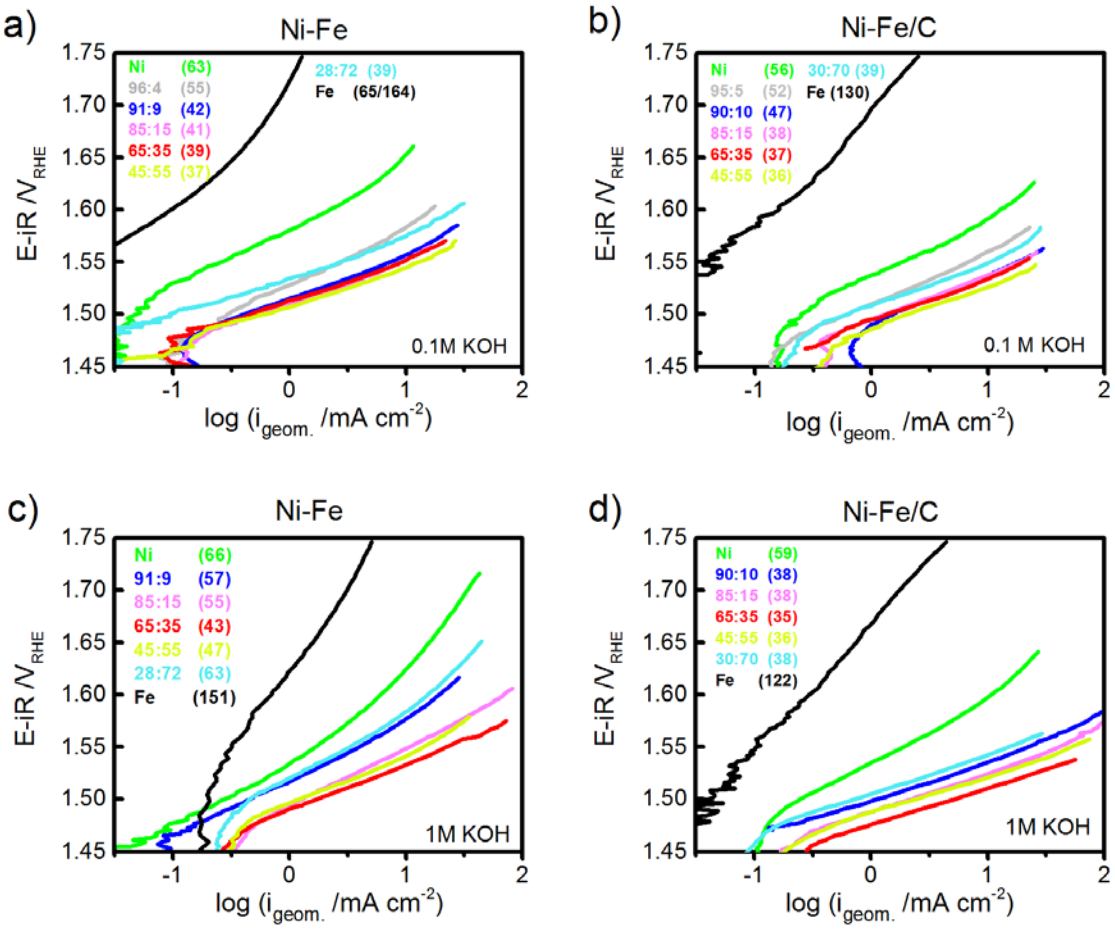

Figure S3. Tafel slopes of Ni-Fe and Ni-Fe/C catalysts with different Ni:Fe compositions. **a)** Unsupported Ni-Fe catalysts in 0.1 M KOH **b)** Carbon supported Ni-Fe/C catalysts in 0.1 M KOH **c)** Ni-Fe catalysts in 1 M KOH **d)** Ni-Fe/C catalysts in 1 M KOH. Atomic compositions of Ni:Fe indicated in the legends were determined by ICP-OES. Tafel slopes are given in brackets after the compositions. Tafel slopes were estimated from CVs measured at a scan rate of 2 mV/s at a rotation speed of 2200 rpm, as the average of the anodic and the cathodic scan.

Stability performance

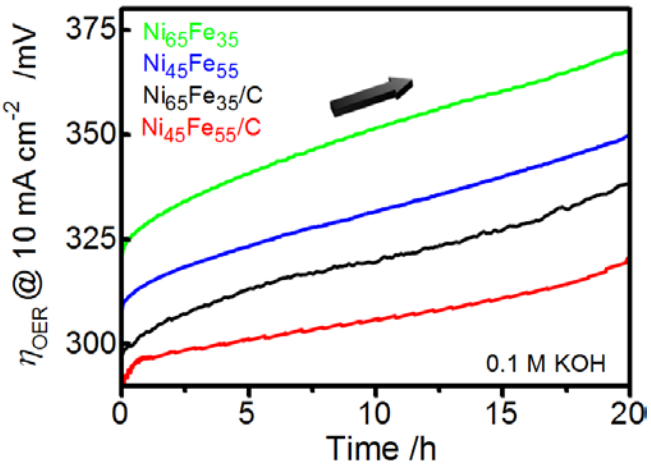

Figure S4. Chronopotentiometric stability measurements at 10 mA cm^{-2} for 20 h, in 0.1 M KOH; of the $Ni_{65}Fe_{35}$, $Ni_{65}Fe_{35}$/C and $Ni_{45}Fe_{55}$, $Ni_{45}Fe_{55}$/C catalysts. The measurements were carried out at a rotation speed of 2200 rpm at a metal loading of ~10 µg cm^{-2} of Ni+Fe.

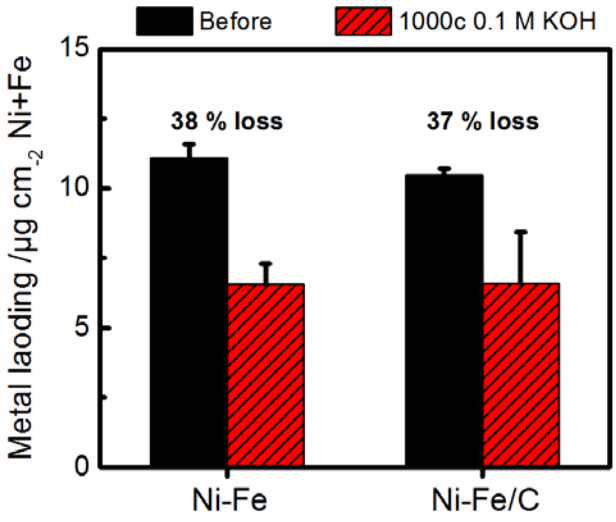

Figure S5. Total metal loadings of Ni+Fe of the unsupported $Ni_{45}Fe_{55}$ and carbon supported $Ni_{45}Fe_{55}$/C catalysts before and after 1000 cycles by cycling between ~1 and 1.6 V_{RHE} (after iR-comp). The measurements were carried out on glassy carbon electrodes in 0.1 M KOH at an initial metal loading of ~10 µg cm^{-2} of Ni+Fe. The metal loading before the measurement and after 1000 potential cycles, determined by TXRF analysis. The errors bars are shown as standard errors estimated from three electrodes.

3.2.1. Catalyst Loading Effects on the OER Activity

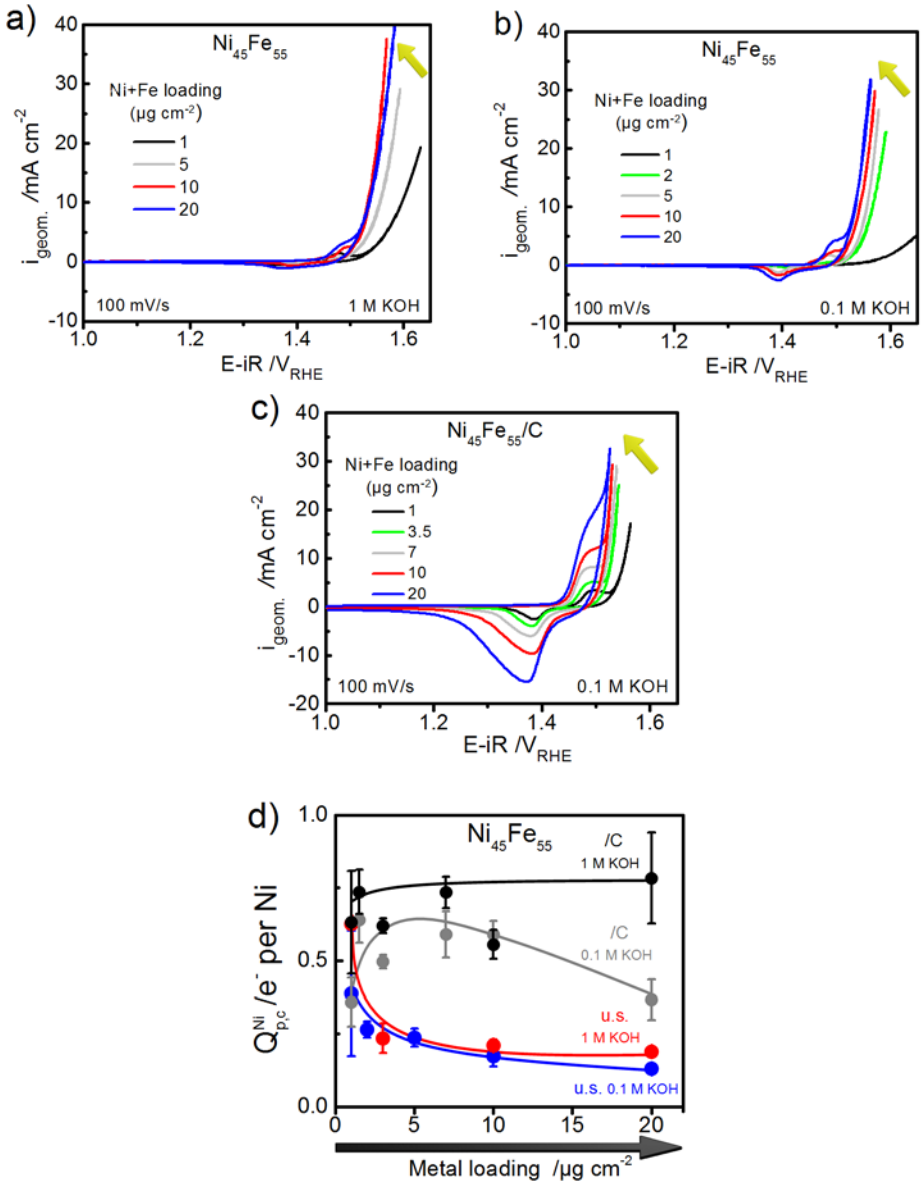

Figure S6. Measurements at different catalyst metal loadings ranging from 1-20 μg cm^{-2} of Ni+Fe. **(a)** CVs of unsupported $Ni_{45}Fe_{55}$ catalyst in 1 M KOH. **(b)** CVs of $Ni_{45}Fe_{55}$ in 0.1 M KOH. **(c)** CVs of the carbon supported $Ni_{45}Fe_{55}$/C catalyst in 0.1 M. **(d)** Redox electrons (e^- per Ni) for the $Ni^{+2} \rightarrow Ni^{+3/+4}$ redox transition, estimated from the cathodic peak ($Q_{p,c}^{Ni}$), from CVs measured at scan rate of 10 mV/s. Catalyst compositions and metal loadings were determined by ICP-OES.

S3.3. DEMS-Derived Charge Efficiency during Oxygen Evolution

Online Head Space Mass Spectrometry & Gas Chromatography

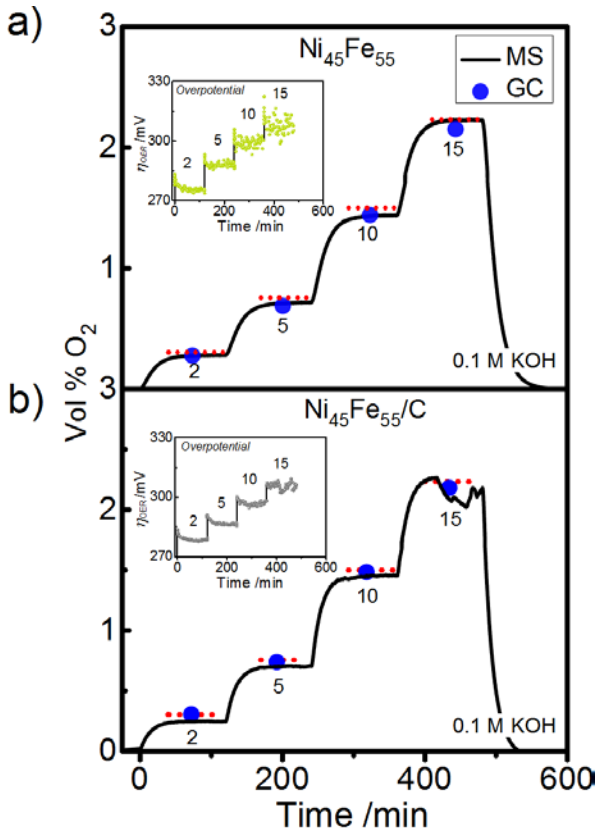

Figure S7. Online headspace mass spectrometry (HS-MS) measured in a gas tight cell setup in a steady flow of 5 sccm of N_2. **(a)** Unsupported $Ni_{45}Fe_{55}$ catalyst measured in 0.1 M KOH. **(b)** Carbon supported $Ni_{45}Fe_{55}$/C catalyst in 0.1 M KOH. Chronopotentiometric (CP) steps were applied in between 2-15 mA cm^{-2}, each step was held for 2h. The MS was continuously sampling in the headspace in the gas outlet of the cell, shown as the molar volume % (Vol %) of O_2 *(black curves)*. Samples were regularly taken out manually and analyzed using Gas chromatography (GC) to confirm the MS detected levels *(blue dots)*. The theoretical levels of O_2 in the given N_2 flow are shown *as red dotted lines*. A carbon fiber paper (CFP) was applied as working electrode (~2 cm^2) with a catalyst loading of 30 µg cm^{-2} of Ni+Fe. The insets show the corresponding overpotentials during the measurements.

Table S1. a) List of K** values used for conversion of the mass spectrometric ion current to corresponding Faradaic current. **b)** Faradaic efficiencies of O_2 (*m/z* 32) obtained from online mass spectrometry presented in Figure S7.

a)

K** (m/z 32)	**0.1 M KOH**	**0.5 M KOH**	**1 M KOH**
$Ni_{45}Fe_{55}$	$1.75 \cdot 10^{-7}$	$1.88 \cdot 10^{-7}$	$1.74 \cdot 10^{-7}$
$Ni_{45}Fe_{55}$/C	$5.18 \cdot 10^{-8}$	$6.50 \cdot 10^{-8}$	$6.25 \cdot 10^{-8}$

b)

$i_{geom.}$ /mA cm^{-2}	**Faradaic efficiency (%)**			
	$Ni_{45}Fe_{55}$		**$Ni_{45}Fe_{55}$/C**	
	MS	**GC**	**MS**	**GC**
2	93	98	96	98
5	95	97	98	98
10	96	98	99	98
15	99	98	99	97

Faradaic Efficiency by Exclusion of the Redox Wave

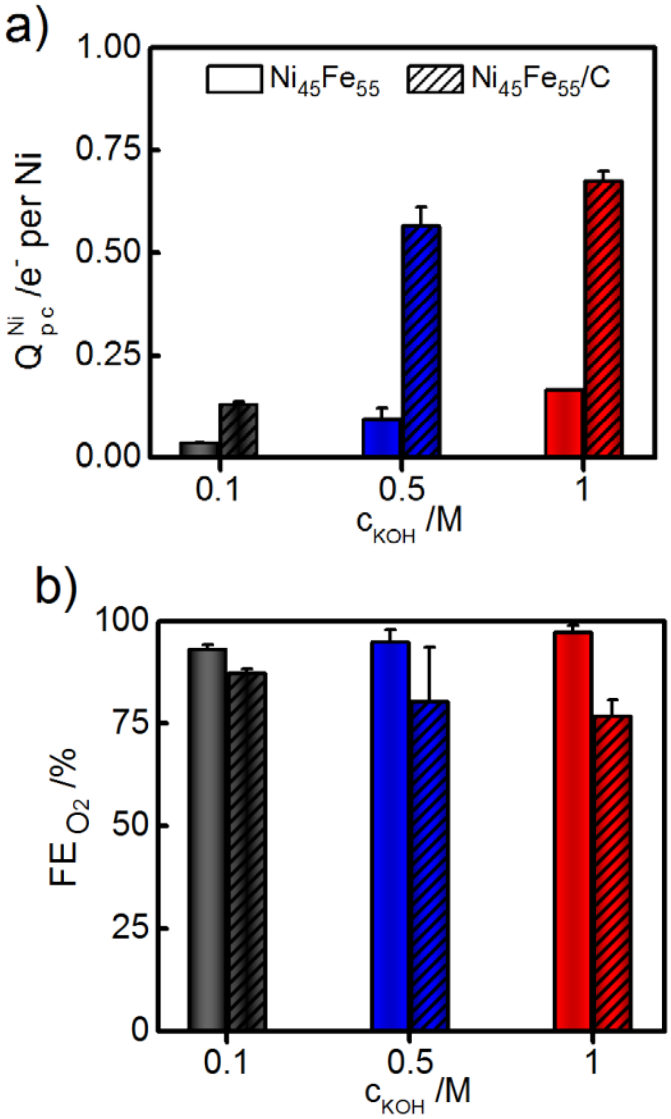

Figure S8. (a) Redox electrons for the cathodic $Ni^{+2} \rightarrow Ni^{+3/+4}$ redox peak ($Q_{p,c}^{Ni}$) extracted from DEMS experiments measured at a scan rate of 10 mV/s in 0.1 M, 0.5 M, and 1 M KOH. **(b)** Faradaic efficiency of O_2 (FEO_2) after subtracting the area from the corresponding redox peak shown in (a). The legend in (a) also applies to (b); Unsupported $Ni_{45}Fe_{55}$ catalysts are shown as *solid bars* and carbon supported Ni-Fe/C catalysts as *hatched bars*.

DEMS-Detection of CO_2 (m/z 44)

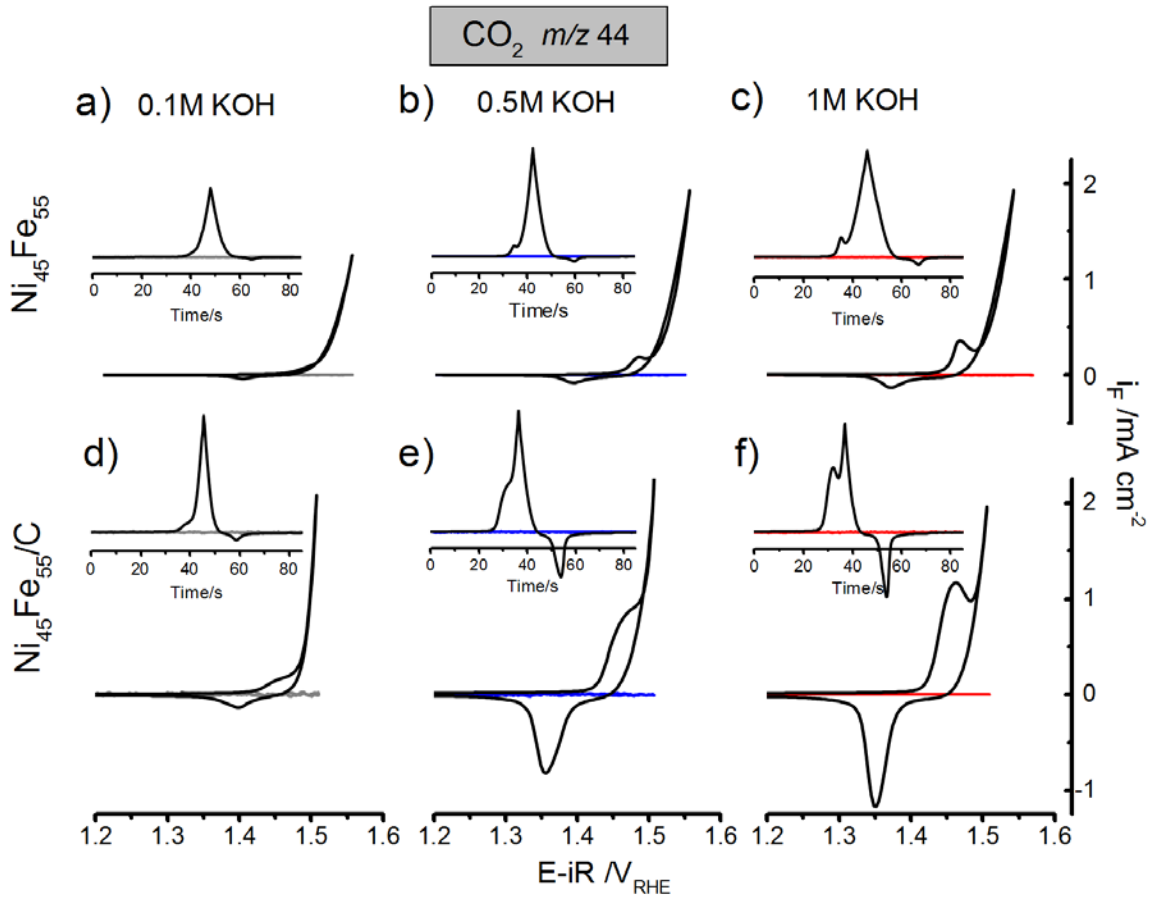

Figure S9. CVs from the DEMS measurements for CO_2 (*m/z* 44), measured at a scan rate of 10 mV/s. **(a-c)** unsupported $Ni_{45}Fe_{55}$ catalyst in 0.1 M KOH (gray), 0.5 M KOH (blue) and 1 M KOH (red); **(d-f)** Carbon supported $Ni_{45}Fe_{55}$/C catalysts in the corresponding electrolytes presented in (a-c). The current densities at the potentiostat (i_F) are shown as black curves and the mass spectrometric detected faradaic ion currents of m/z 44 ($i_{F,CO2}^{DEMS}$) are shown as colored lines.

3.4. Tracking Metal Redox States Using *In Situ* UV-vis spectroscopy

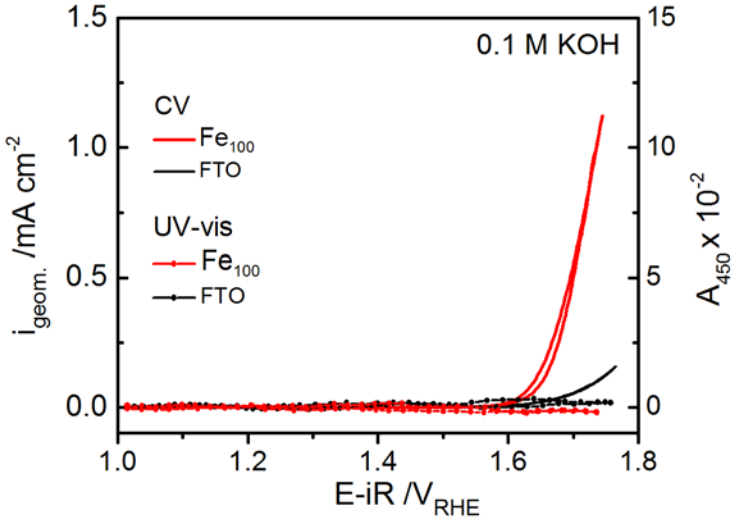

Figure S10. UV-vis spectroelectrochemistry of unsupported Fe(OOH) catalyst and an empty FTO electrode without catalyst during CV cycling at 10 mV/s in 0.1 M KOH. The absorption band at 450 nm (A_{450}) is shown on the right axis and the current density ($i_{geom.}$) on the left axis. The absorption is shown as an average of the wavelengths between 400-500 nm to reduce the noise. The catalyst loading was kept at 5 µg cm^{-2}, determined by TXRF analysis.

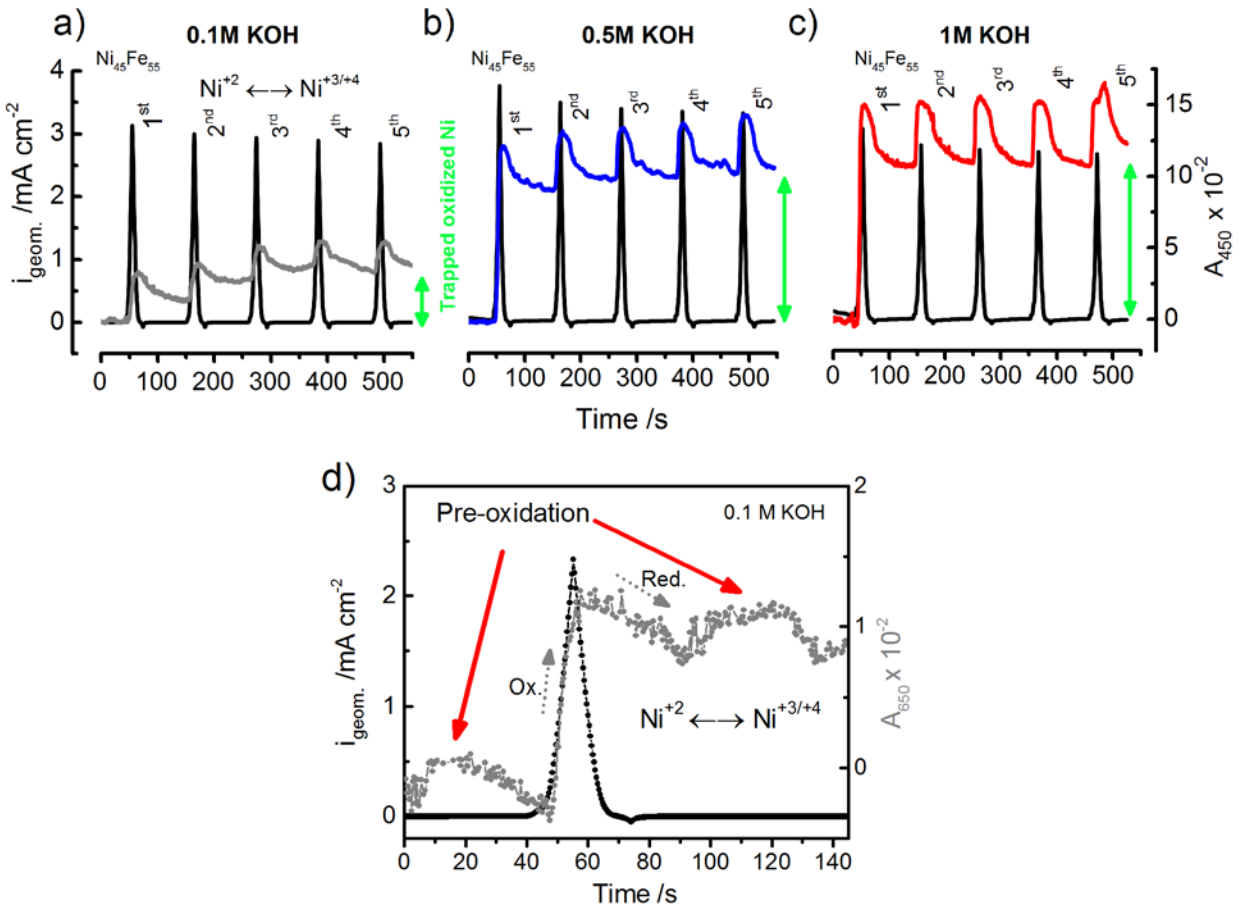

Figure S11. UV-vis spectroelectrochemistry of unsupported $Ni_{45}Fe_{55}$ catalyst. The absorption band at 450 nm is shown in the time domain during 5 potential cycles in **a)** 0.1 M KOH **b)** 0.5 KOH and **c)** 1 M KOH. Before starting the measurement, all catalysts were exposed to a reducing potential of 0 V_{RHE} for 2 min in order to reduce oxidized Ni centers and bring the absorption baseline back to zero. **d)** Time trace of $Ni_{45}Fe_{55}$ during a CV scan at (1^{st} cycle), showing the presence of an unknown oxide species (pre-oxidation wave), arising before the $Ni^{+2} \rightarrow Ni^{+3/+4}$ oxidation. The time trace is shown at 650 nm. The catalyst loadings were kept constant at 5 µg cm^{-2} of Ni, determined by TXRF analysis.

Quasi-Stationary State Potential Steps

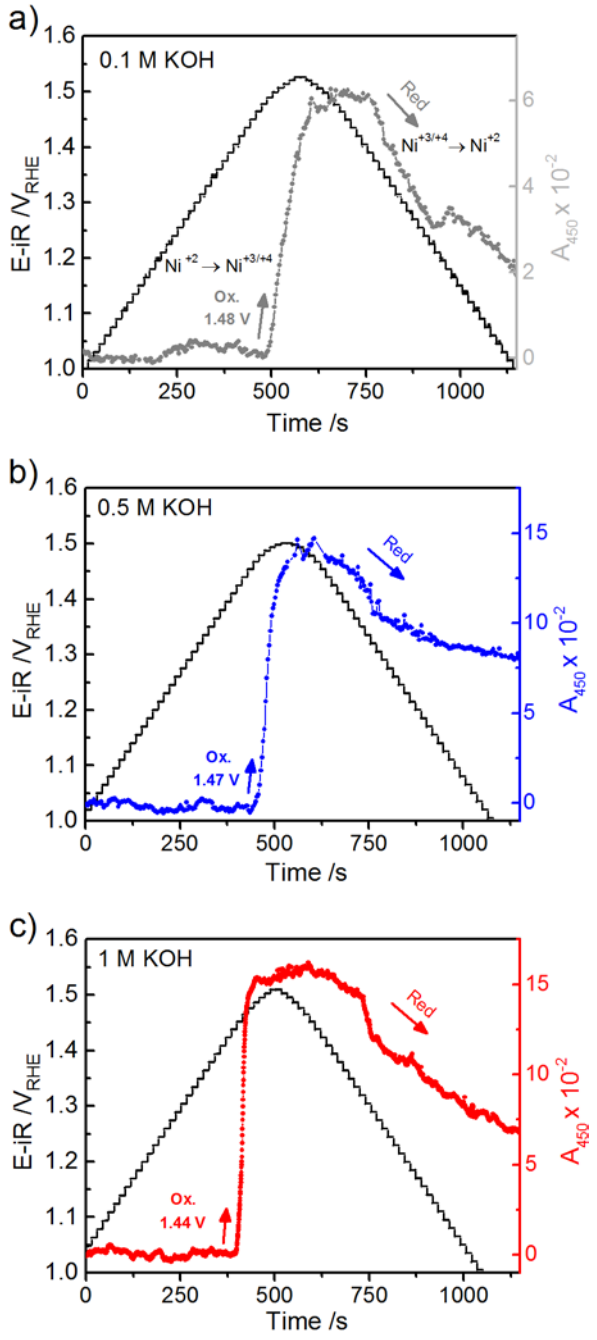

Figure S12. UV-vis spectroelectrochemistry of unsupported $Ni_{45}Fe_{55}$ catalyst in 0.1, 0.5 and 1 M KOH. Potential steps were applied for 15 sec in each steps. The absorption was monitored at 450 nm, assigned to the oxidation process $Ni^{+2} \rightarrow Ni^{+3/+4}$. The time traces are shown as an average of the wavelengths between 400-500 nm. The catalyst loadings were kept constant to 5 µg cm^{-2} of Ni, determined by TXRF analysis.

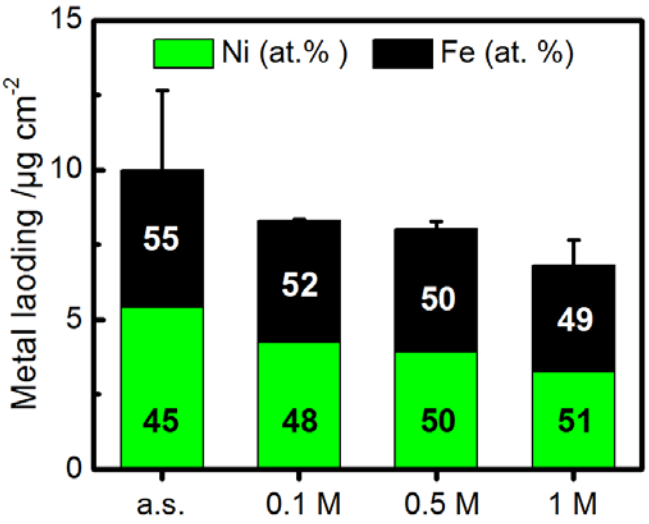

Figure S13. Total metal loading of Ni+Fe determined by TXRF analysis for the unsupported $Ni_{45}Fe_{55}$ catalyst investigated according to the UV-vis measurements protocol. The measurements were carried out on FTO electrodes by consecuetive cycling in 0.1→ 0.5 M → 1 M KOH. The labels indicate which pH the catalyst was latest exposed to before analyzed.

3.5. Non-Nernstian pH Effects and Decoupled Proton-Electron Transfer

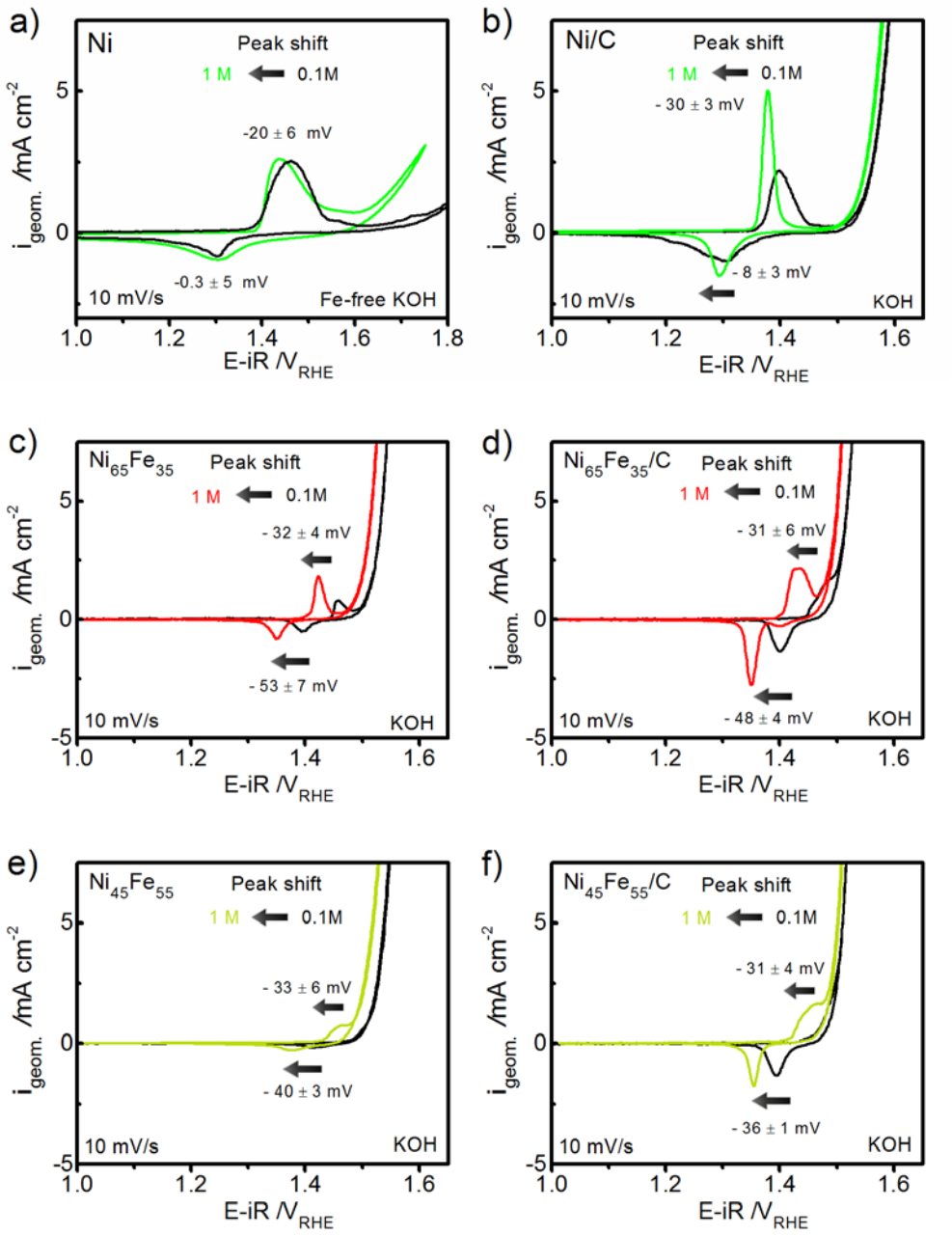

Figure S14. CVs measured in 0.1 M and 1 M KOH at a scan rate of 10 mV/s. **(a)** Unsupported Ni catalyst **(b)** Carbon supported Ni/C catalyst **(c)** $Ni_{65}Fe_{35}$ **(d)** $Ni_{65}Fe_{35}$/C **(e)** $Ni_{45}Fe_{55}$ **(f)** $Ni_{45}Fe_{55}$/C. The CVs were collected at a rotation speed of 1600 rpm at a geometric metal loading of 5-10 µg cm^{-2} of Ni+Fe, determined by ICP-OES. The Ni and Ni/C catalysts may contain Fe impurities.

3.6. Local Atomic Structure under Catalytic OER Conditions

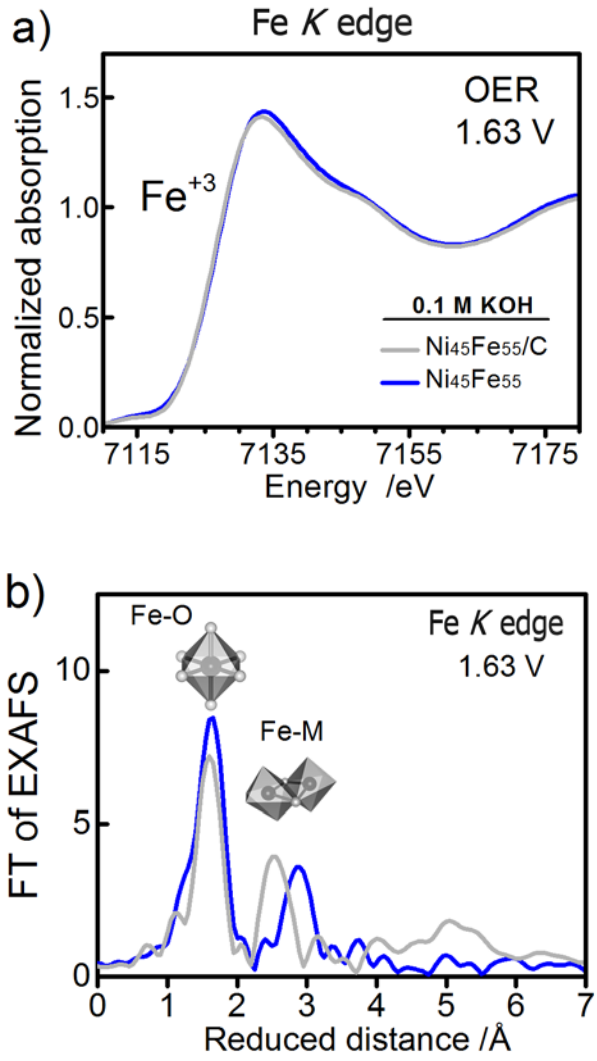

Figure S15. X-ray absorption spectroscopy (XAS) measured at the Fe *K*-edge of the $Ni_{45}Fe_{55}$ and $Ni_{45}Fe_{55}$/C catalysts freeze quenched under catalytic potential of 1.63 $V_{RHE.}$ **(a)** Fe *K*-edge XANES. (**b)** k^3-weighted FT-EXAFS. The catalysts were freeze quenched at 1.63 V_{RHE} in 0.1 M KOH after a pre-conditioning step of 30 min. Catalyst compositions are given as at. %, determined by ICP-OES.

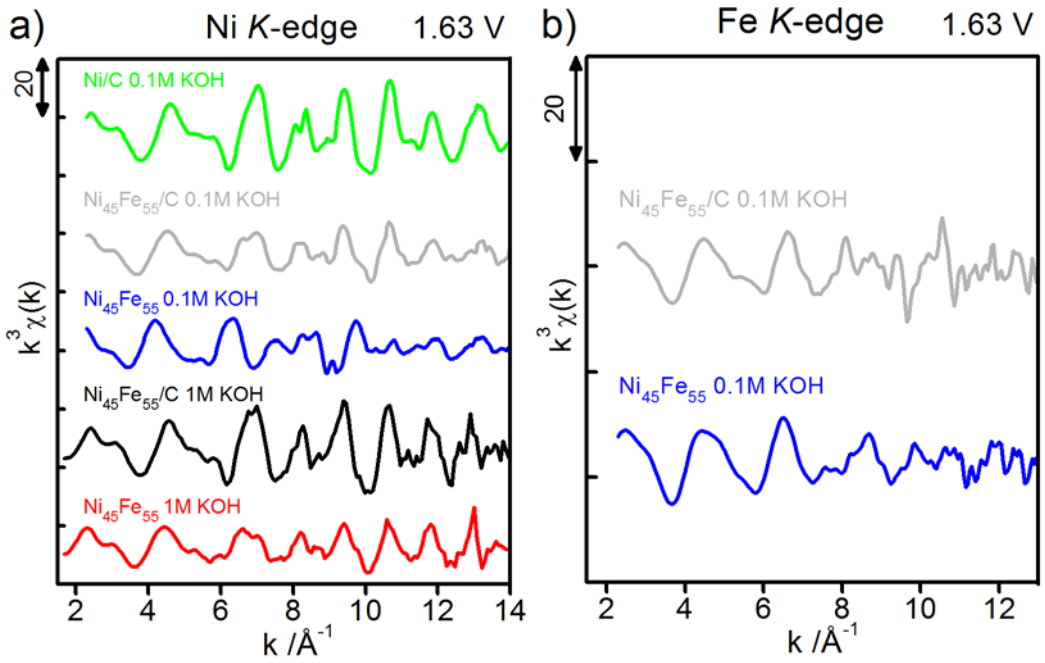

Figure S16. Extended X-ray absorption fine structure (EXAFS) of the unsupported $Ni_{45}Fe_{55}$ and carbon supported Ni/C and $Ni_{45}Fe_{55}$/C catalysts, freeze quenched at 1.63 V_{RHE} in 0.1 M or 1 M KOH after a pre-conditioning step of 30 min at the given potential. **(a)** Ni *K*-edge spectra (**b)** Fe *K*-edge spectra. Catalyst compositions are given as at. %, determined by ICP-OES. (*) The Ni catalyst may contain Fe impurities.

Table S2. Ni *K*-edge simulation fit parameters of Ni/C, unsupported $Ni_{45}Fe_{55}$ and carbon supported catalysts $Ni_{45}Fe_{55}$/C catalysts in 0.1 M and 1 M KOH, at catalytic potential of $1.63V_{RHE}$.

Catalyst	Shell	R (Å)	N	σ (Å)	R_f
Ni/C	Ni-O (short)	1.88 ± 0.01 [c]	5.3 ± 0.7	0.07 ± 0.01	19.9
0.1M KOH	Ni-M (short)	2.81 ± 0.01 [d]	6.7 ± 1.0	0.06 ± 0.01	
	Ni-M (double short)	5.63 [†]	3.1 ± 0.8	0.06 ± 0.01	
$Ni_{45}Fe_{55}$/C	Ni-O (short)	1.88 ± 0.01 [c]	5.1 ± 1.0 [e]	0.09 ± 0.02	25.7
0.1M KOH	Ni-O (long)	2.04 ± 0.01 [a]	0.9 ± 1.0 [e]	0.09 ± 0.02	
	Ni-M (short)	2.81 ± 0.01 [d]	4.5 ± 0.4 [f]	0.08 ± 0.01	
	Ni-M (long)	3.08 ± 0.01 [b]	1.5 ± 0.4 [f]	0.08 ± 0.01	
	Ni-M (double short)	5.63 [†]	2.8 ± 1	0.08 ± 0.01	
$Ni_{45}Fe_{55}$	Ni-O (long)	2.04 ± 0.01 [a]	5.6 ± 0.5	0.07 ± 0.01	24.8
0.1M KOH	Ni-M (long)	3.08 ± 0.01 [b]	3.3 ± 0.1	0.06 ± 0.01	
	Ni-M (double long)	6.16 [†]	1.3 ± 0.5	0.06 ± 0.01	
$Ni_{45}Fe_{55}$/C	Ni-O (short)	1.88 ± 0.01 [c]	5.1 ± 0.6	0.05 ± 0.02	23.1
1 M KOH	Ni-M (short)	1.88 ± 0.01 [d]	4.7 ± 0.8	0.05 ± 0.02	
	Ni-M (double short)	5.63 [†]	1.9 ± 0.7	0.05 ± 0.02	
$Ni_{45}Fe_{55}$	Ni-O (short)	1.88 ± 0.01 [c]	3.5 ± 0.5 [g]	0.05 ± 0.02	31.0
1 M KOH	Ni-O (long)	2.04 ± 0.01 [a]	2.5 ± 0.5 [g]	0.05 ± 0.02	
	Ni-M (short)	2.81 ± 0.01 [d]	3.7 ± 0.4 [h]	0.07 ± 0.01	
	Ni-M (long)	3.08 ± 0.01 [b]	2.3 ± 0.4 [h]	0.07 ± 0.01	
	Ni-M (double short)	5.63 [†]	1.6 ± 1	0.07 ± 0.01	

Values for which no fit error is shown were not fitted.

[*] The Ni catalyst may contain Fe impurities. Long Ni-O [(a)], long Ni-M [(b)], short Ni-O [(c)], and short Ni-M [(d)] distances had the same values in the four models in a joint-fit approach. Double Ni-M distances [(†)] were set equal to the (dominating) single Ni-M distance multiplied by two. The double-distance Ni-M shells included multiple-scattering contributions. The sums of the coordination numbers of the short and long Ni-O shells in $Ni_{45}Fe_{55}$ in 0.1 M KOH [(e)] and $Ni_{45}Fe_{55}$ in 1MKOH [(g)] models were set to 6. The sums of the coordination numbers of the short and long Ni-M shells for $Ni_{45}Fe_{55}$ in 0.1M KOH [(f)] and $Ni_{45}Fe_{55}$ in 1MKOH [(h)] models were set to 6. Debye-Waller parameters of the Ni-O and the Ni-M shells had the same values within the models.

Table S3. Fe *K*-edge simulation fit parameters of Ni/C, unsupported $Ni_{45}Fe_{55}$ and carbon supported catalysts $Ni_{45}Fe_{55}$/C catalysts in 0.1 M KOH, at catalytic potential of $1.63V_{RHE}$.

Catalyst	Shell	R (Å)	N	σ (Å)	R_f
$Ni_{45}Fe_{55}$/C	Fe-O	1.98 ± 0.02	5.1 ± 0.6	0.09 ± 0.01 [c]	
0.1M KOH	Fe-M (short)	2.93 ± 0.02 [a]	3.5 ± 1.9	0.08 ± 0.04 [d]	18.0
	Fe-M (long)	3.11 ± 0.02 [b]	2.1 ± 1.3	0.08 ± 0.04 [d]	
$Ni_{45}Fe_{55}$/C	Fe-O	2.00 ± 0.01	5.2 ± 0.8	0.08 ± 0.01 [c]	
0.1M KOH	Fe-M (short)	3.08 ± 0.01 [a]	3.7 ± 0.5	0.08 ± 0.01 [d]	17.9
	Fe-M (long)	3.45 ± 0.02 [b]	0.3 ± 0.8	0.08 ± 0.01 [d]	

The short Fe-M [(a)] and long Fe-M [(b)] distances had the same values in the three models in a joint-fit approach.

Debye-Waller parameters of the Fe-O shells [(c)] and the two Fe-M shells [(d)] had the same values in the three models.